Dislocation dynamics in Rayleigh–Bénard convection

Th. Walter and W. Pesch[a)]
Physikalisches Institut der Universität Bayreuth, D-95440 Bayreuth, Germany

E. Bodenschatz
Laboratory of Atomic and Solid State Physics, Cornell University, Ithaca, New York 14853

(Received 19 January 2004; accepted 24 May 2004; published online 16 September 2004)

Theoretical results on the dynamics of dislocations in Rayleigh–Bénard convection are reported both for a Swift–Hohenberg model and the Oberbeck–Boussinesq equations. For intermediate Prandtl numbers the motion of dislocations is found to be driven by the superposition of two independent contributions: (i) the Peach–Koehler force and (ii) an advection force on the dislocation core by its self-generated mean flow. Their competition allows to explain the experimentally observed bound dislocation pairs. © *2004 American Institute of Physics.*
[DOI: 10.1063/1.1772231]

In many situations nonequilibrium transitions in nature lead to striped patterns. These are typically not perfect and various types of defects sustain a specific persistent dynamics. In particular, dislocations, i.e., the topological point defects where stripes terminate in the interior of the system, play an important role. Here we study various aspects of the dynamics of dislocations in Rayleigh–Bénard convection, which is one of the best investigated paradigms among pattern forming systems. We interpret the dislocation dynamics in terms of two competing forces, one of which corresponds roughly speaking to an energy minimization principle (Peach–Koehler force) while the other is mediated by a long-range mean flow (or pressure) field. This leads, for instance, to a natural explanation of the experimentally observed bound dislocation pairs. Our approach can be expected to transcend the particular example of Rayleigh–Bénard convection, as different pattern forming systems share a commonality, which is most clearly captured in familiar model equations, like the Swift–Hohenberg equation used here.

I. INTRODUCTION

Striped patterns are ubiquitous in nature. They are found in physical, chemical, and biological systems, which are driven away from equilibrium.[1] In general natural patterns are not perfect due to the presence of defects, like grain boundaries (line defects) and topological point defects (dislocations).[2] The nucleation, motion, and annihilation of dislocations is essential for many pattern-selection processes, which are initiated by modulational instabilities.[1] Dislocations govern the ordering kinetics of initially disordered patterns[3] and sustain in defect turbulent systems the perpetual reordering of the plan forms.[4] Though much effort has been devoted to their study (see, e.g., Refs. 1 and 5–11 and references therein), a detailed understanding of the dislocation dynamics, especially in the presence of nonlocal interactions, remains a challenge. Dislocations present a simple realization of topological singularities in a field description of continuous extended systems. To which extent their dynamics can be understood in terms of quasiparticles subject to effective forces is a general important issue beyond the field of pattern formation.[12]

In this paper we present a numerical study of the dislocation dynamics in Rayleigh–Bénard convection (RBC), which is a main paradigm for pattern forming instabilities in isotropic systems.[13] By using both the full hydrodynamic equations and standard, well accepted model equations we show that dislocations are driven by a superposition of two independent ''forces.'' One is the well known Peach–Koehler (PK) force, which describes the tendency of the system to develop towards a striped pattern with an optimal average wave number.[5,8] This concept has been at first introduced in solid state physics to describe the dislocation dynamics under the influence of an external stress,[14] which is crucial to understand the strength of crystals. The second force, an ''advection force,'' is due to a long-range pressure field caused by strong roll curvature gradients in the vicinity of a dislocation, which excite a flow field with a finite vertical average (mean flow).[15] We demonstrate that the advection force acts in general to remove dislocations from the system so as to reduce the wave number of the pattern. For a certain wave number q_D the two forces balance and a single dislocation is stationary. In the vicinity of q_D two approaching dislocations of opposite topological charge can form bound states which have been observed before in experiments.[16,17] Although the significance of the mean flow had been expected for a long time in line with experiments,[18] its direct identification in a previous theoretical analysis had failed.[19]

In Sec. II we review some basic facts about dislocations and sketch our numerical procedures. Section III is the central part of this paper. We present the numerical results that allow a natural interpretation in terms of the PK and advection force. The bound state of two dislocations demonstrated in Sec. IV is a natural consequence of this concept. In Sec. V we have added some comments on the stability of disloca-

a)Electronic mail: werner.pesch@uni-bayreuth.de

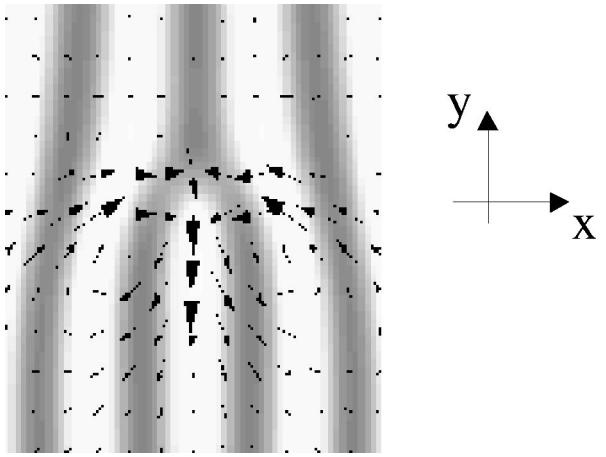

FIG. 1. Temperature field (gray scale) in the presence a dislocation with positive topological charge $Q=2\pi$ and the superimposed mean-flow velocity field (arrows) shown at the midplane of the fluid layer; from simulations of the OBE for $\epsilon\equiv(R-R_c)/R_c=0.3$, $\sigma=1.2$, and background wave number $\overline{q}=q_c$. The dislocation is moving downwards along the y axis, while it would move upwards if $Q=-2\pi$.

tions. The paper concludes with some final remarks (Sec. VI).

II. THEORETICAL BACKGROUND AND NUMERICAL PROCEDURE

In RBC a horizontal layer of a simple fluid is heated from below and cooled from above, where conventionally the Rayleigh number R serves as the dimensionless measure of the applied temperature gradient.[13] For R above the threshold R_c buoyancy driven convection is observed in the form of striped convection roll patterns with the critical wave number $q=q_c$. The strength of the mean flow is determined by the relative distance $\epsilon=(R-R_c)/R_c$ to the threshold and in particular by the Prandtl number $\sigma=\nu/\kappa$, with the kinematic viscosity ν and the thermal diffusivity κ. Intermediate Prandtl numbers ($\sigma\sim1$) are realized in gas convection experiments.[13] In RBC the full hydrodynamic description [Oberbeck–Boussinesq equations (OBE)] is well established and the theoretical analysis can be quantitatively compared with well controlled experiments.[13] The commonality of RBC with other bulk pattern-forming systems is most clearly expressed in well known model equations, like the Swift–Hohenberg (SH) equation[20] and its generalizations.[21] In Fig. 1, a snapshot of the midplane temperature field $\Psi(x,y)$ containing a dislocation with positive topological charge $Q=2\pi$ from simulations of the OBE is shown. Q is defined via the winding number of the phase gradient $\nabla\Phi(x,y)$ of Ψ around a dislocation with the two possibilities $\oint\nabla\Phi(x,y)ds=\pm2\pi$. The mean flow (arrows) is maximal at the dislocation core and tends to advect the dislocation downwards along the symmetry axis. In the direction perpendicular to the plane shown in Fig. 1 the mean flow shows an almost perfect parabolic profile.

While a comprehensive exploration of the R,σ parameter space within the OBE is extremely time consuming, we have gained much insight into the basic physical mechanism of dislocation dynamics by first studying the standard two-dimensional generalized SH equations (GSH):[1,8,21]

$$\partial_t\Psi+(\mathbf{U}\cdot\nabla)\Psi=[\epsilon_S-(1+\nabla^2)^2]\Psi-\Psi^3, \tag{1}$$

$$\mathbf{U}=(U_x,U_y)=(\partial_y\xi,-\partial_x\xi), \tag{2}$$

$$(\partial_t-\nabla^2+c)\nabla^2\xi=g(\nabla(\nabla^2\Psi)\times\nabla\Psi)\cdot\mathbf{e}_z. \tag{3}$$

In terms of the two-dimensional field $\Psi(\mathbf{x},t)$ the GSH equations describe (in suitable dimensionless units) the bifurcation to patterns with critical wave number $q_c=1$ and their nonlinear saturation. ϵ_S measures the relative distance to onset. The vertical average of the mean drift (or mean flow) $\mathbf{U}(\mathbf{x})$ is determined by a velocity potential ξ. The coupling of ξ and Ψ is characterized by a coupling constant g (in RBC $g\propto1/\sigma$) and a cutoff parameter c ($c=2$ in this work). Note, that the mean flow $\mathbf{U}(\mathbf{x})$ is associated with the vertical vorticity $-\Delta\xi$. For $g=0$ the present GSH equations derive from a Lyapunov functional $\mathcal{L}$.[1]

In our numerical analysis we focused on dislocation climb, i.e., the motion parallel to the roll axis as shown in Fig. 1, in a rectangular domain $-L_{x,y}/2<x,y<L_{x,y}/2$ with width L_x and length $L_y=2L_x$. We solved both the GSH and the OBE equations numerically by a pseudospectral method with semi-implicit time stepping.[22] In order to minimize finite-size effects, we initially simulated dislocation pairs with periodic boundary conditions in the x,y directions (Fig. 1 has to be extended mirror symmetrically along the y axis). We found, however, almost identical results for the less expensive simulations with a single dislocation in a box kept finite in the y direction by gradually ramping ϵ to zero at $y=\pm L_y/2$. The ideal periodic roll pattern of wavelength $\lambda=2\pi/q$ without an immersed dislocation consisted of up to $N=64$ roll pairs, corresponding to $L_x=N\lambda$. The typical numerical resolution was $\geqslant16$ grid points per wavelength. It is crucial to study systematically the defect dynamics as a function of the background wave number $\overline{q}$ of the underlying pattern. A superimposed dislocation leads to $N+1$ roll pairs in some parts of the cell (see Fig. 1, below the dislocation) and consequently to a reduced wavelength $\lambda_+=N/(N+1)\lambda$ and thus to a wave number $q_+=2\pi/\lambda_+>q$. We found that defining the background wave number as $\overline{q}=(q_++q)/2$ was most effective to absorb the finite N corrections. In designing the details of our calculation scheme and to validate our GSH code we have considerably benefitted from the comparison with Ref. 8, devoted to the GSH model.

III. PEACH–KOEHLER VERSUS ADVECTION FORCE

In this section we present numerical results mainly from GSH equations but also from the OBE equation. The analysis of the data leads naturally to the notion of two forces acting on a climbing dislocation, namely the PK force in competition with an advection force.

The simulations are initialized with a single dislocation at the center $\mathbf{r}_0=(x_0,y_0)=(0,0)$ by an approximate ansatz $\Psi(x,y,t=0)\propto\cos[qx-\phi(|\mathbf{r}|)]$. Here $\phi(r)$ is the polar angle about $\mathbf{r}_0$. After the initial transients died out (typically after the dislocation core has moved about four wavelengths λ in

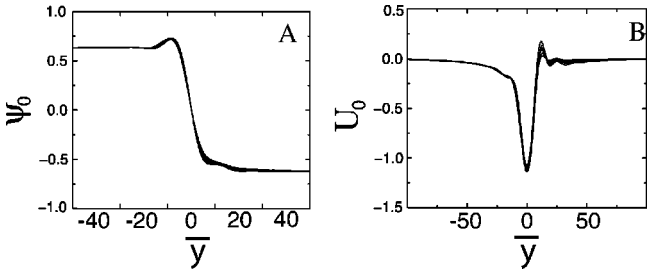

FIG. 2. Profiles of $\Psi_0(\overline{y})\equiv\Psi(x_0,\overline{y})$ and $U_0(\overline{y})\equiv U_y(x_0,\overline{y})/g$ plotted along the roll axis centered about the dislocation core at $(x_0=0,\overline{y}=y-v_{st}t=0)$ obtained from GSH simulations at $\epsilon_S=0.3$ and $\overline{q}=0.98$ in the range $2<g<20$ for $N=16$. The profiles cover 100 pixels (A) and 200 pixels (B) of the calculation grid of 512 pixels along $\overline{y}$, where 16 grid points correspond to a wavelength $\lambda=2\pi/q$.

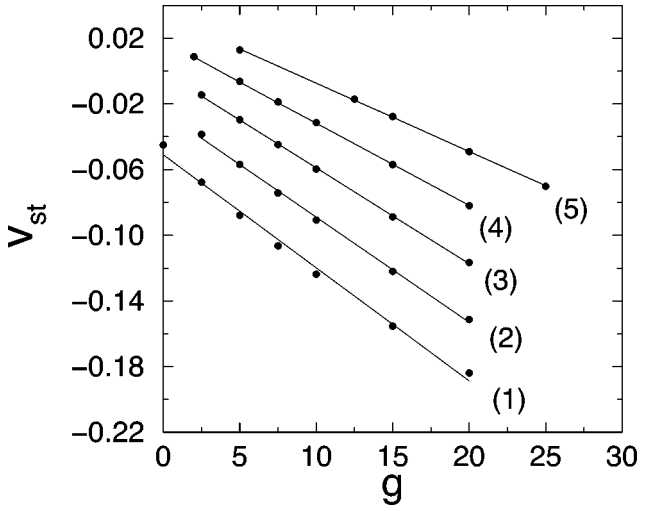

FIG. 3. Dislocation velocity from GSH simulations as function of the mean flow strength g at $\epsilon_S=0.3$, $N=16$, for various $\overline{q}$: (1) 1.04, (2) 1.02, (3) 1.00, (4) 0.98, and (5) 0.96. The linear fits of the data serve as a guide for the eye.

Fig. 1) the dislocation would climb with a constant velocity v_{st} and a relaxed asymptotic shape $\Psi(x,y,t)=\Psi(x,y-v_{st}t)$ is reached. Starting from this state in subsequent runs, considerably reduced the computational time. In agreement with prior investigations,[8,11] we have identified a wave number $q_D(\epsilon,g)$, such that for $\overline{q}>q_D$ the dislocation climbed downwards with $v_{st}<0$ (the case shown in Fig. 1), while it moved upward for $\overline{q}<q_D$.

The key for the physical interpretation of the numerical results lies in a certain universality of Ψ and $\mathbf{U}$ for a dislocation, which climbs uniformly along the symmetry axis $x=x_0=0$ (see Fig. 1). As demonstrated in Fig. 2 the solutions $\Psi(x_0,\overline{y})\equiv\Psi_0(\overline{y})$ with $\overline{y}=(y-v_{st}t)$ of Eq. (1) at *fixed* background wave number are virtually identical although the mean-flow coupling g varies over a wide range. Note that data for $g<2$ are not available, but there is no reasonable doubt that the limiting case $g\to 0$ is covered.[23] When the source term for ξ in Eq. (3) is evaluated with Ψ_0 the explicit linear dependence on g prevails. Thus it is not surprising [see Fig. 2(B)] that the (suitably rescaled) mean flow component $U_y(x_0,\overline{y})/g$ along the symmetry axis has practically a g-independent shape $U_0(\overline{y})$. Note that the transverse component U_x vanishes for symmetry reasons at $x=x_0$.

According to the discussion above the field Ψ on the symmetry axis is very well approximated by the $g\to 0$ limit of Ψ_0. Thus on the symmetry axis Eq. (1) reduces to

$$-v_{st}\partial_{\overline{y}}\Psi_0(\overline{y})=-\frac{\delta\mathcal{L}}{\delta\Psi_0(\overline{y})}-(U_y\partial_{\overline{y}})\Psi_0(\overline{y}). \tag{4}$$

Integrating the three terms in Eq. (4) separately over $\overline{y}$ about the dislocation core at $\overline{y}=0$ leads thus to the following relation for v_{st} as function of $\overline{q}$ and g:

$$v_{st}(\overline{q},g)=v_{PK}(\overline{q})+gU_0^M c_1(\overline{q}). \tag{5}$$

Here we have rewritten the $\overline{y}$ average of the mean-flow contribution in Eq. (4) in terms of the minimum gU_0^M of $U_y=gU_0$ at the dislocation core ($\overline{y}=0$), where $\partial_{\overline{y}}\Psi_0(\overline{y})$ is also strongly peaked [see Fig. 2(A)]. The quantities v_{PK},c_1, which are determined by the practically g-independent profile Ψ_0, must be calculated numerically as a function of $\overline{q}$ and ϵ_S.

For clarity the two contributions to v_{st} on the right hand side of Eq. (5) are discussed for $Q=2\pi$ (see Fig. 1), since the case $Q=-2\pi$ is analogous. The PK force leads to the g-independent velocity contribution v_{PK}, which is negative for $\overline{q}>q_{opt}\approx q_c$, vanishes for $\overline{q}=q_{opt}$, and becomes positive for $\overline{q}<q_{opt}$. Thus for $g=0$ the dislocation climbs as to adjust the wave number of the pattern in its wake towards $\overline{q}=q_{opt}$. The second term $\propto g$ on the right hand side of Eq. (5) originates from an advection force on the dislocation due to its self-generated mean flow U_y. It is not difficult to deduce from the GSH model Eq. (1) (and also from inspection of Figs. 1 and 2) that the direction of the mean flow and of the ensuing advection force depends only on the topological charge Q of the dislocation. As a result the mean flow tends in general to advect the dislocation in order to decrease the wave number $\overline{q}$.[24] In our GSH simulations the PK force corresponds, in fact, to the minimization of the Lyapunov potential $\mathcal{L}$. This potential property has, however, not been exploited in the discussion before, when we isolated v_{PK} as the $g\to 0$ contribution to v_{st}.

The competition of the Peach–Koehler and the advection force is elucidated in Fig. 3 where we present the velocity of an isolated dislocation as a function of g and $\overline{q}$. Consistent with prior investigations[8] our numerical results show that v_{st} varies almost linearly as a function $\overline{q}$ like $v_{st}\propto(\overline{q}-q_D(g))$ for fixed $g>0$ and $\epsilon_S>0$. According to Eq. (5) this implies at fixed $\overline{q}$ a linear dependence of v_{st} on g as confirmed in Fig. 3 for a wide g range. Extrapolation of the straight lines towards $g=0$ in Fig. 3 yields the Peach–Koehler limit $v_{st}\equiv v_{PK}$ as function of q. We find indeed that v_{PK} vanishes at $q_D\approx q_c=1$ in this limit. With increasing g the negative advection force comes into play and the values of q_D determined by the condition $v_{st}=0$ become increasingly smaller than q_c. For instance a dislocation as shown in Fig. 1 on a background pattern with $\overline{q}=0.96$ would move upward ($v_{st}>0$) for $g=0$, but downwards for $g>10$.

Although the full hydrodynamics (OBE) cannot be rigorously mapped on the GSH, the reasoning in terms of a PK

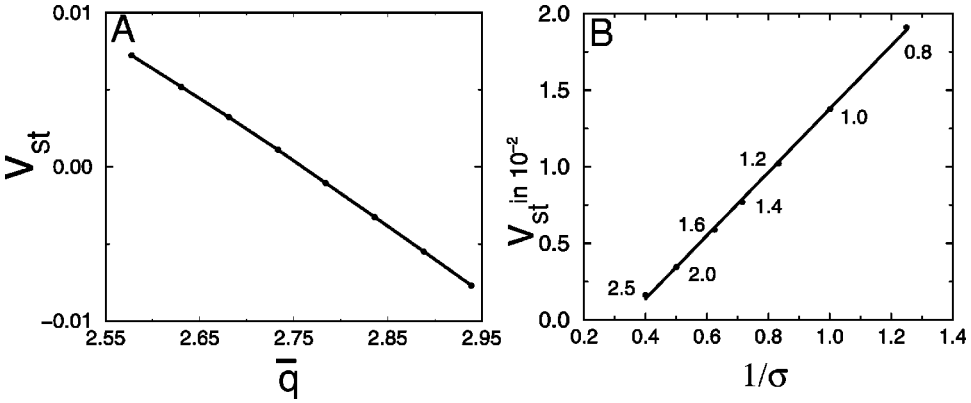

FIG. 4. Dislocation velocity v_{st} in units of $10^{-2}h/t_v$, with h the cell height, and $t_v=h^2/\kappa$ the vertical diffusion time: (A) as function of $\overline{q}$ at fixed $\sigma=1.4$ and (B) as function of σ in the range $0.8\leqslant\sigma\leqslant 2.5$ at $\overline{q}=2.91$; data from simulations of the OBE for $\epsilon=0.3$.

force ($\sigma\to\infty$) and a competing mean flow force seems to apply as well. As a typical example for $\sigma=1.4$, we show in Fig. 4(A) the linear variation of $v_{st}(\overline{q})\propto(\overline{q}-q_D)$, where v_{st} crosses zero at $\overline{q}=q_D=2.75$. This behavior is in perfect agreement with the experimental and numerical analysis of the dynamics of the off center "giant spirals"[11] for $\sigma\approx 1$ where the orbiting outer dislocations probe roll patches in a fairly large $\overline{q}$ range. Our results are at variance with a $v\propto((\overline{q}-q_D)^{3/2}$ law as favored in Ref. 7 to describe RBC defect dynamics for $\sigma\approx 1$. As already mentioned in Ref. 8 such a law cannot be justified for nonpotential models. In line with the GSH it is demonstrated in Fig. 4(B) that v_{st} varies indeed linearly in $\sigma^{-1}\sim g$ at fixed $\overline{q}$.

IV. BOUND STATE OF DISLOCATIONS

The notion of the advection force, which has been introduced in Sec. III, is supported by the observation of bound states of dislocations in our numerical simulations. Although bound states have been observed more than a decade ago in gas convection experiments at medium Prandtl numbers σ,[16,17] they had not found a theoretical explanation.

As a representative example from our OBE simulations the stationary configuration of two dislocations with separation l_D is shown in Fig. 5(a). The bound state, which shows an additional roll segment between the dislocations, has developed when we seeded two dislocations of opposite charge Q at a distance $L>l_D$ on a background pattern with $\overline{q}\gtrsim q_D=2.75$. Analogous bound states have been found in our more detailed investigations of the GSH equations as well. The equilibrium distance l_D of the bound dislocations as function of $\overline{q}$ and g, or σ, respectively, has not been investigated systematically. Typically we find $l_D\sim 2-3\lambda$. A systematic, certainly difficult stability analysis of the bound state was not attempted; we tested, however, that the equilibrium state would also develop from a dislocation pair with an initial distance $L<l_D$. An experimental example of a bound state in a giant spiral is shown in Fig. 5(b), which was destroyed after a long period by an increase of the background wave number $\overline{q}$ away from q_D.

The existence of bound states can be easily rationalized from Eq. (5). A well separated pair of oppositely charged dislocations is driven by the dominant mean-flow contribution $\propto|U_0^M|$ in Eq. (5) towards their annihilation. However, this advection force weakens continuously, as the opposing mean flow contributions from each dislocation begin to overlap destructively. The velocities diminish and eventually the dislocations stop moving, when the reduced advection force is balanced by the opposing PK force. To our surprise even the deceleration of the approaching dislocations was well captured adiabatically by Eq. (5), though derived under the assumption of constant v_{st}. The velocity v of the approaching dislocations, which decreases continuously with their distance L [see Fig. 6(a)], remains indeed directly proportional to U_0^M at either dislocation core [see Fig. 6(b)].

V. STABILITY OF DISLOCATIONS

In our OBE and GSH simulations dislocations are found to be very robust objects except when $\overline{q}$ was in the vicinity of a cross-roll (CR) instability boundary of the Busse

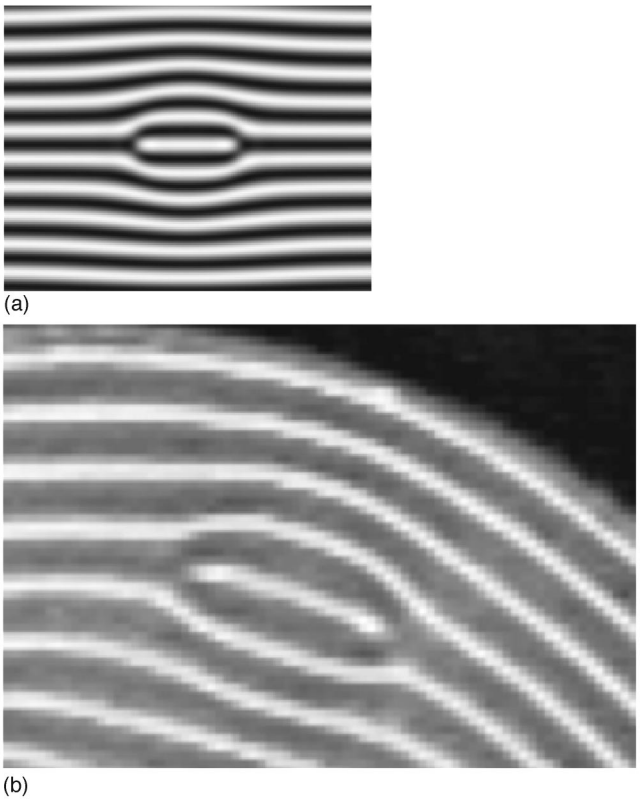

FIG. 5. Stationary bound state from OBE simulations $\epsilon=0.3,\sigma=1.4,N=16$, for $\overline{q}=2.8$ [upper panel (a)] and experimental bound state in section of a giant spiral at $\epsilon=0.7,\sigma=1.4$ (Ref. 17) [lower panel (b)].

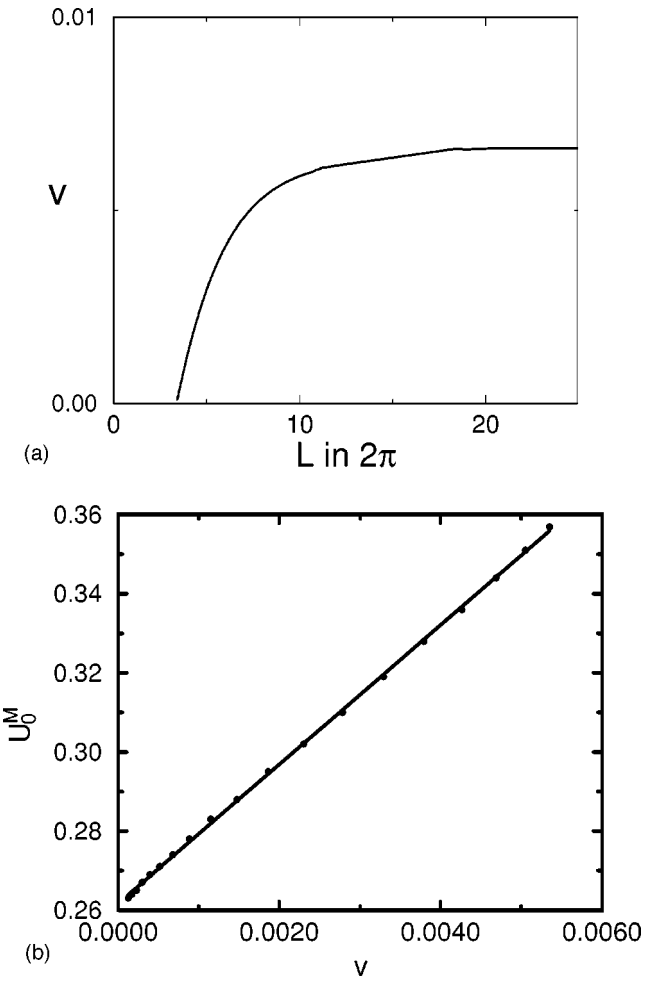

FIG. 6. Velocity v of two approaching dislocations in the GSH model as a function of their instantaneous distance L [upper panel (a)]; mean flow U_0^M at the dislocation core as function of v [lower panel (b)]; simulations at $g=5$, $\epsilon=0.3$, and $\overline{q}=0.98$

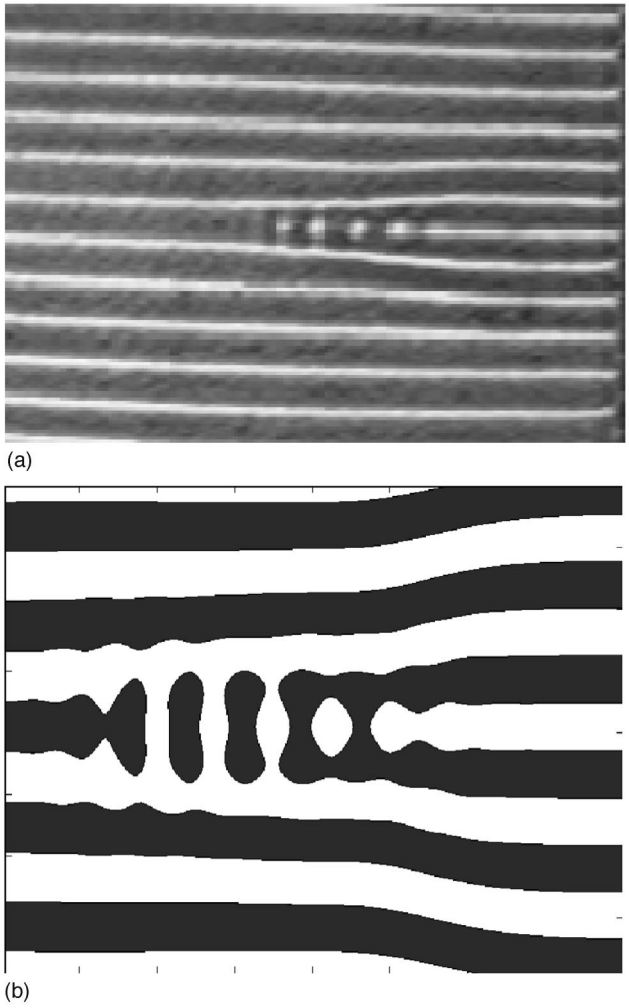

FIG. 7. Bridges developing in front of a dislocation moving to the left (Pr $=1.09, \epsilon=0.7, q=2.3$) [experiment (Ref. 13), upper panel (a)] and in OBE simulations (Pr$=1.4, \epsilon=0.3, q=2\pi\lambda=2.425$) [lower panel (b)] near cross-roll instability at $q=2.385$.

balloon[25] for ideal roll. A typical experimental snapshot is shown in Fig. 7(a), where a dislocation, moving from the right into a pattern with $q<q_D$, seems to split into a chain of ''bubbles.'' In analogous OBE simulations [Fig. 7(b)] it is obvious that the bubbles develop from localized transverse bridging of adjacent rolls. The phenomenon of a splitting of the dislocation core has been described at first in GSH-model simulations[10] for $g=0$ in perfect agreement with our own simulations. In Ref. 10 a generic instability of a dislocation towards the splitting into disclinations has been invoked. In contrast we favor an interpretation in terms of a local CR instability, which is nucleated by the finite perturbation due to the dislocation.[26] In fact, in all our OBE and GSH simulations core splitting has been observed exclusively in the vicinity of a CR instability line of the corresponding Busse balloons.

The excitation of local CRs by a dislocation is also reflected in regular oscillations of its velocity in time. A representative example is shown in Fig. 8. A dislocation was seeded at time $t=0$ into striped patterns with different q. An initial steep increase of the velocity v due to the relaxation of the seeded dislocation is followed by oscillations. Their number and intensity increases with decreasing distance of q to the CR instability q_{cr} (from the upper to the lower curve in Fig. 8). Only for the lower curve was a persistent generation of local CRs and bubbles observed for a longer period. However, eventually the CRs extended over many rolls and the original pattern was globally reorganized.

Besides the short wavelength CR instability of a roll pattern with wave vector $\mathbf{q}=(q,0)$ the Busse balloon is in addition organized by modulational instabilities with wave vector $\mathbf{s}=(s_x,s_y)$ with $s \ll q$. The case $s_x=0$ denotes the zig-zag (ZZ), the case $s_y=0$ the Eckhaus instability, while the general case $s_x, s_y \neq 0$ corresponds to the skewed varicose instability.[25] The case $s_y \neq 0$ is reflected in characteristic undulations along the stripes, which are inevitably nucleated by the strong perturbations of a dislocation.

In Fig. 9(a) the case of a ZZ unstable pattern is shown. Since $q<q_D \approx 1$ in this case, the dislocation tends to penetrate the pattern. However, it does not climb along a straight path, but is almost perfectly guided by the undulations. This is demonstrated in Fig. 9(b), where the trajectory of the dislocation follows closely the undulations of the stripes. The dynamics involves thus a combination of climb along the roll axis and glide perpendicular. For completeness we mention

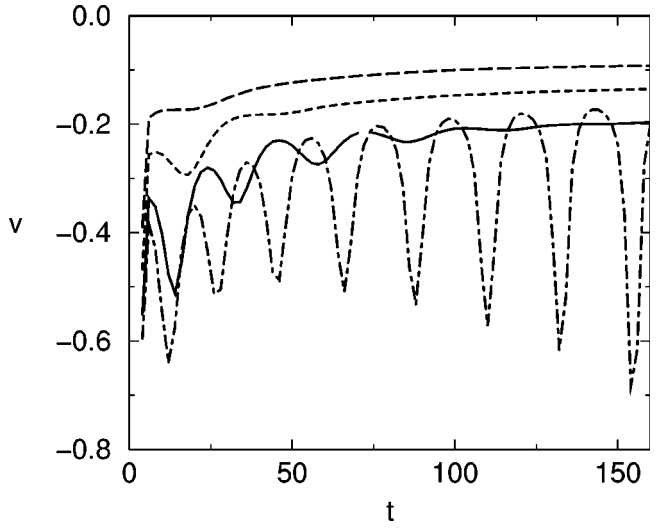

FIG. 8. Dislocation velocity v as function of time in a GSH simulation ($N=16, \epsilon=0.3$) near the CR instability line ($q=1.164$) for increasing q: $q=1.1$ (upper long-dashed curve); $q=1.12$ (short-dashed); $q=1.14$ (solid); $q=1.15$ (dashed dotted).

that in the case of a SV instability the dislocation moves into a direction perpendicular to **s**. So far, an appropriate theoretical modeling of combined climb and glide dynamics is missing.

VI. CONCLUSIONS

We have reported numerical experiments on RBC at intermediate Prandtl numbers with particular emphasis on the dynamics of dislocations. The theoretical analysis led us to the identification of two driving forces: the PK force due to the short scale pattern mode (Ψ) and the long-range advection forces driven by a mean flow (ξ) with its large scale contributions. There is hope that these considerations might also help to get a better intuitive picture of the intriguing dislocation dynamics in the presence of ramps in the Rayleigh number.[27] We expect that our methodology will be applicable to a number of other systems as well. Striped patterns are observed in a large variety of extended continuum systems, for example, in Taylor–Couette flow,[1] gas discharges,[28] and in vertically vibrated granular layers,[29] where the mean drift ($\equiv$vorticity) plays an important role in the defect dynamics, although an appropriate continuum model has yet to be constructed. In binary fluid convection ξ corresponds to a concentration mode,[30] which allows bound states of fronts in analogy to our bound dislocations. As a last example we mention patterns observed in block polymers, which have have been described by a SH model coupled to a flow field as well.[31]

ACKNOWLEDGMENTS

E.B. is grateful for support from the National Science Foundation (NSF) under Grant Nos. DMR 0072077 and DMR 030515. E.B. and W.P. would also like to acknowledge support from NSF Grant No. PHY99-07949 during the program *Pattern Formation in Physics and Biology* at the Kavli Institute for Theoretical Physics, University of California at Santa Barbara, where the work was completed. We (W.P. and E.B.) dedicate this paper to Lorenz Kramer. For many years Lorenz has been a good friend. We have very fond memories of his leadership during excursions, including mountain climbing with W.P., hiking with the group, paragliding and white water canoeing with E.B. From his deep insights into physics we have benefited a lot in joint work. His persistent quest for the understanding of topological defects has always been contagious as reflected already in investigations on vortices in superconductivity with W.P. in the early 1970s. In the mid 1980s, when E.B. was a graduate student at Bayreuth, Lorenz wrote with us a well accepted paper about defect dynamics in anisotropic pattern forming systems.[11] Many of the ideas presented here have their roots in those beginnings.

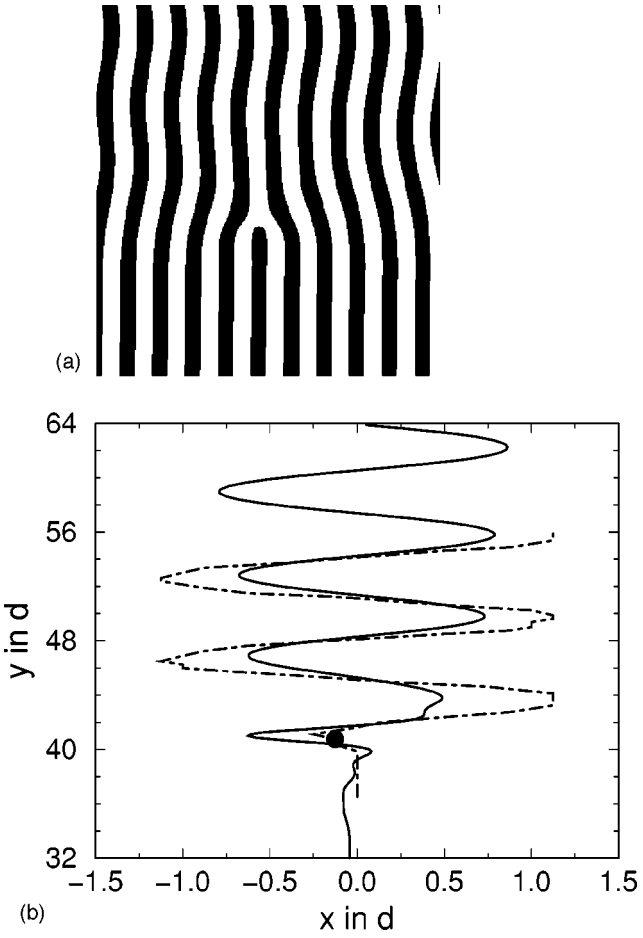

FIG. 9. Snapshot of a dislocation moving along the y axis ($q<q_D$) into a ZZ unstable background pattern; from an OBE simulation at $\epsilon=0.3$, $\sigma=20$, $q=2.85$, and $N=32$ [upper panel (a)]. The trajectory of a dislocation (dashed-dotted line) in the $x-y$ plane in units of the roll diameter $d=\pi/q$ [lower panel (b)]. The instantaneous undulations of convection roll in front of the dislocation (solid line) recorded at the dislocation position marked by the black dot are superimposed.

[1] M. C. Cross and P. C. Hohenberg, Rev. Mod. Phys. **65**, 851 (1993) and references therein.
[2] A. C. Newell, T. Passot, and J. Lega, Annu. Rev. Fluid Mech. **25**, 399 (1993).
[3] C. Harrison *et al.*, Science **290**, 1558 (2000); L. Purvis and M. Dennin, Phys. Rev. Lett. **86**, 5898 (2001).

[4] K. Daniels and E. Bodenschatz, Phys. Rev. Lett. **88**, 034501 (2002) and references therein.
[5] E. D. Siggia and A. Zippelius, Phys. Rev. A **24**, 1036 (1981).
[6] Y. Pomeau, P. Manneville, and S. Zaleski, Phys. Rev. A **27**, 2710 (1983).
[7] A. Pocheau and V. Croquette, J. Phys. (France) **45**, 35 (1984).
[8] G. Tesauro and M. C. Cross, Phys. Rev. A **34**, 1363 (1986).
[9] E. Bodenschatz, W. Pesch, and L. Kramer, Physica D **32**, 135 (1986).
[10] A. C. Newell and T. Passot, Phys. Rev. Lett. **68**, 1846 (1992).
[11] B. Plapp, D. Egolf, E. Bodenschatz, and W. Pesch, Phys. Rev. Lett. **81**, 5334 (1998).
[12] L. M. Pismen, *Vortices in Nonlinear Fields* (Clarendon, Oxford, 1999).
[13] E. Bodenschatz, W. Pesch, and G. Ahlers, Annu. Rev. Fluid Mech. **32**, 709 (2000) and references therein.
[14] M. Peach and J. S. Koehler, Phys. Rev. **80**, 436 (1950).
[15] See, e.g., K. H. Chiam, M. R. Paul, M. C. Cross, and H. S. Greenside, Phys. Rev. E **67**, 056206 (2003).
[16] E. Bodenschatz *et al.*, Physica D **61**, 77 (1992).
[17] B. Plapp, Ph.D. thesis, Cornell University, Ithaca, NY, 1997.
[18] A. Whitehead, J. Fluid Mech. **75**, 715 (1976).
[19] See the discussion in Ref. 5, where the OBE were solved, however, in a fairly small system with unrealistic free-slip boundary condition.
[20] J. Swift and P. C. Hohenberg, Phys. Rev. A **15**, 319 (1977).
[21] P. Manneville, J. Phys. (Paris) **44**, 759 (1983); H. S. Greenside and W. M. Coughran, Phys. Rev. A **30**, 398 (1984).
[22] W. Pesch, Chaos **6**, 348 (1996).
[23] The limit $g=0$ could not been achieved in our simulations, since for $\overline{q}=0.98$ the dislocations would excite the ZZ instability resulting in undulated stripes and in a modified dynamics (see Fig. 9). In fact, it is evident from Fig. 3 that all v_{st} curves extrapolate continuously to $g=0$.
[24] In more technical terms the coefficient $c_1(\overline{q})$ in Eq. (5) was found to be always positive for all $\overline{q}$ and ϵ_S.
[25] F. H. Busse, Rep. Prog. Phys. **41**, 1929 (1978).
[26] The simulations in Ref. 10 were performed right at the CR instability line ($q_{\mathrm{cr}}=1.5>q_c$ for $\epsilon_S=3$). It should also be mentioned, that in our larger integration domain with controlled initial conditions, we found no indication of a resonant $q/3$ process.
[27] K. M. S. Bajaj, N. Mukolobwiez, N. Currier, and G. Ahlers, Phys. Rev. Lett. **83**, 5282 (1999).
[28] Y. A. Astrov, I. Müller, E. Ammelt, and H.-G. Purwins, Phys. Rev. Lett. **80**, 5341 (1998).
[29] J. R. de Bruyn, C. Bizon, M. D. Shattuck, D. Goldman, J. B. Swift, and H. L. Swinney, Phys. Rev. Lett. **81**, 1421 (1998).
[30] H. Herrero and H. Riecke, Physica D **85**, 79 (1995).
[31] T. Ohtai and K. Kawasaki, Macromolecules **19**, 2621 (1986); P. Chen and J. Vinals, *ibid.* **35**, 4183 (2002).